RSC Advances

PAPER

View Article Online
View Journal | View Issue

Cite this: *RSC Adv.*, 2020, **10**, 5428

Bond-photon-phonon thermal relaxation in the M(X, X_2) (M = Mo, Re, Ta, Ge, Sn; X = S, Se, and Te)

Yonghui Liu,[ab] Hongwei Xiao,[ab] Li Luo[ab] and Huayun Xiao *[ab]

Received 8th December 2019
Accepted 21st December 2019

DOI: 10.1039/c9ra10288d

rsc.li/rsc-advances

We systematically investigated the temperature-dependent bandgap energy and Raman shift on the bond length and bond energy, Debye temperature, and atomic cohesive energy for M(X, X_2) *via* bond relaxation methods. It is revealed that the thermal decay of both bandgap energy and phonon frequency arose from the thermal integration of the specific heat of Debye approximation. The results indicate that (i) the bandgap energy relaxation is due to the thermal excitation-induced weakening of the bond energy, and the phonon frequency was just a function of bond length and bond energy; (ii) the Debye temperature determines the nonlinear range at low temperatures; (iii) the reciprocal of the atomic cohesive energy governs the linear behavior at high temperatures. Thus, the outcomes of this study include fundamental information about photon, phonon, and the thermal properties of layered semiconductors, which are crucial to develop the new generations of thermal and electronic applications of devices based on layered semiconductors.

1. Introduction

During the last two decades, numerous studies have focused on two-dimensional (2D) nanomaterials because graphene sheets[1] have been produced *via* mechanical exfoliation to obtain unusual physical and chemical properties. More recently, graphene-like 2D nanomaterials such as metal chalcogenides and phosphorene have attracted significant interest as they can be used to manufacture new or improved field-effect transistors,[2–4] optoelectronic devices,[5–7] and topological superconductors.[8–10] Metal chalcogenides, include metal dichalcogenides and metal monochalcogenides, whose chemical formulae are MX and MX_2, respectively, where M represents a metal atom of molybdenum (Mo), tantalum (Ta), rhenium (Re), germanium (Ge) or tin (Sn); and X stands for atoms of either sulfur (S), selenium (Se), or tellurium (Te). MX has wrinkled honeycomb structures, similar to phosphorene, which shows an ultralow thermal conductivity. MX_2 has a hexagonal honeycomb structure that exhibits unique electronic properties. This makes it a promising candidate material with diverse applications such as batteries,[11,12] field-emission devices,[13] and thermoelectric energy conversion.[14,15] Hence, studying the properties of these 2D ultrathin films can have far-reaching benefits for future semiconducting devices.

The availability of a wide range of bandgaps is very beneficial for both fundamental research and semiconductor applications. A crystal of $MoTe_2$, which belongs to the family of metal dichalcogenides, is a semiconductor with an indirect bandgap of about 1.0 eV.[16] It transitions to a direct-bandgap semiconductor with an optical gap of 1.10 eV (ref. 17) when used as a monolayer. Moreover, nanomaterials based on $ReSe_2$, $SnSe_2$, SnS_2, and $GeSe_2$ show strong covalent bonds within very weak interlayer interactions. This means that the bandgap type of bulk material is the same as that of the monolayer. For example, bulk materials consisting of $ReSe_2$, $SnSe_2$ and SnS_2 are indirect bandgap semiconductors with gaps of 0.92 eV (ref. 18), 1.07 eV (ref. 19), and 2.18 eV (ref. 19), respectively. However, their respective monolayer counterparts show increasing indirect bandgaps with gaps of 1.22 eV (ref. 18), 1.69 eV (ref. 19), and 2.41 eV (ref. 19). Moreover, the metal monochalcogenides such as SnS, SnSe, and GeSe are indirect bandgap semiconductors with gaps of 1.58 eV (ref. 20), 0.83 eV (ref. 21), and 1.04 eV (ref. 22), respectively. The suitable bandgaps not only expand the application range of these 2D films but also increase the interest in the study of their fundamental thermodynamic properties. For instance, the thermal excitation effects with respect to the optical bandgaps of monolayers and bilayers of $MoTe_2$ were measured with a 125 and 50 μW laser powers.[23] Furthermore, as the temperature increases the gaps of these films, a red-shift was observed. The bandgap energy of the layered SnS films was also investigated for temperatures between 20 K and 200 K (ref. 24), and the results reveal a similar shift toward lower energies. However, Varshni's semiempirical relationship[25,26] can generally describe the observation that the bandgap energies shift toward lower energy with increasing temperature, which is a consistent understanding of the bond and photon attributes and hence their correlation remain in their infancy.

Furthermore, it is important to note that the self-heating of the device is unavoidable. In particular, when both bias and back-gate voltages are applied, the device performance can

[a]*Jiangxi Province Key Laboratory of the Causes and Control of Atmospheric Pollution, East China University of Technology, Nanchang, 330013, China. E-mail: xiaohuayun@ecit.cn*

[b]*College of Water Resources and Environmental Engineering, East China University of Technology, Nanchang, 330013, China*

substantially degrade in highly integrated electronic components. Usually, the heat in 2D nanomaterials mainly propagates *via* acoustic phonons,[27,28] which determine its thermal conductivity. Therefore, it is very important to study the temperature dependence of the lattice vibrations of metal chalcogenides as nanomaterials. Raman spectroscopy is a very good method for the *in situ* analysis of both phonon scattering and lattice distortion in the 2D nanomaterials. Therefore, the thermal response of Raman spectroscopy of the 2D materials was measured in some studies. For monolayer $ReSe_2$ (ref. 29), the frequencies of all the observed phonon modes exhibited nonlinear temperature dependence with incident laser wavelengths of 532 nm at low temperatures. Moreover, the temperature-dependent Raman spectroscopy of the SnSe sample[30] shows intrinsic non-harmonic phonon scattering. In general, the temperature dependence of the Raman actives modes of the 2D nanomaterials was analyzed using the Grüneisen[31–34] model, which indicates that the non-harmonic properties are due to the decay of an optical phonon into multiple acoustic phonons. However, the calculation of the nonlinear phonon properties at low temperatures using the Grüneisen model does not agree well with the observations.

In this study, we used a Bond-Order-Length-Strength (BOLS) approximation,[35,36] which intrinsically probes bond–photon–phonon thermal softening properties across a wide temperature range. A simulation of the temperature-dependent bandgap energy and Raman shift of these 2D films revealed valuable quantitative information, including the Debye temperature (θ_D), atomic cohesive energy (E_z), and the referential frequency (ω_L, L denotes A_{1g}, E^1_{2g}, A^3_g, and B_{3g} modes). We confirm that the Debye temperature determines the nonlinear range at low temperatures, while the atomic cohesive energy determines the linear behavior at high temperatures.

2. Principles

2.1. Bond-phonon correlation

It is well-known that a Raman shift can be described using $\omega = \omega(0) + \Delta\omega$. Here, $\omega(0)$ is the Raman frequency of the reference point, and $\Delta\omega$ is the perturbation of the temperature (T) with respect to the Raman frequency. $\omega(0)$ varies with the frequency of the substrate material and the wavelength of the incident light. However, the trend of the perturbation $\Delta\omega$ remains unchanged when thermal excitation is used. According to the interatomic potential function, $u(r)$ can be expanded using a Taylor series around its equilibrium position, and the Raman shift can be derived as:[37]

$$u(r) = \sum_{n=0}\left(\frac{\mathrm{d}^n u(r)}{n!\mathrm{d}r^n}\right)_{r=d_z}(r-d_z)^n = E_{z_i} + \frac{\mu\omega^2(r-d_z)^2}{2} + o\left[(r-d_z)^{n\geq 3}\right] \quad (1)$$

The term ($n = 0$) corresponds to the equilibrium single bond energy at 0 K; the term ($n = 1$) is the force at equilibrium; the term ($n = 2$) corresponds to the thermal vibration energy, which dominates the Raman shift; the term ($n \geq 3$) correspond to the nonlinear vibrations. So, omitting the higher-order terms, one can obtain the following relationship:

$$\frac{1}{2}\Delta\omega^2 x^2 \cong \frac{1}{2}\left.\frac{\partial^2 u(r)}{\partial r^2}\right|_{r=d_z} x^2 \propto \frac{1}{2}\frac{E_z}{\mu \mathrm{d}_z{}^2}x^2 \quad (2)$$

According to eqn (2), the Raman shift (ω) can be described by using $\Delta\omega$, which is a function of bond length (d_z) and bond energy (E_z) in the z^{th} atomic layer for the entire Raman spectroscopy. The $\mu = m_1 m_2/(m_1 + m_2)$ is the reproduced mass of the representative bond.[38] Thus, the Raman shift can be derived as: $\omega(d_z, E_z) = (E_z/\mu)^{1/2}/d_z$.

2.2. Bond-photon correction

The bandgap energy (E_g) can be calculated using the first-order Fourier coefficient of the crystal potential (V_{cry}) function. $E_g = 2|V_1| \propto \langle E_b \rangle$, where the bandgap energy is proportional to the single bond cohesive energy $\langle E_b \rangle$, and $V_1 = \int V_{cry}(r) e^{ik\cdot r}\mathrm{d}r$. Here, $e^{ik\cdot r}$ is the Bloch wave function for equilibrium conditions. This means that the crystal potential function determines the intrinsic bandgap energy E_g. The expression of the bandgap energy for a given perturbation temperature can be written as:

$$E_g(T) = E_g(0)(1 + \Delta_T) \quad (3)$$

here, $E_g(T)$ and $E_g(0)$ represent the bandgap energies at the measured temperature and 0 K, respectively. $\Delta_T \int_{T_0}^{T} \eta(t)\mathrm{d}t$ is the perturbation of temperature with respect to the bandgap energy.

2.3. Bond length and bond energy thermal relaxation

The relationship between the bond length and bond energy for thermal relaxation can be described using the following equation:

$$\begin{cases} d(T) = d_{z_b}\left(1 + \int_{T_0}^{T} o(t)\mathrm{d}t\right) \\ E(T) = E_{z_b}\left(1 - \dfrac{\int_{T_0}^{T}\eta(t)\mathrm{d}t}{E_z}\right) \end{cases} \quad (4)$$

here, $\alpha(t)$ is the thermal expansion coefficient; d_{z_b} and E_{z_b} denote the bond length and bond energy of the film materials without thermal stimuli, respectively. Eqn (4) indicates that the bond length expands, and the bond energy weakens upon stimulation *via* heating for the entire electron and Raman spectrum. The integration of the specific heat $\eta(t)$ can be described by the following relationship:

$$\int_0^T \eta(t)\mathrm{d}t = \int_0^T \frac{C_v(T/\theta_D)}{z_i}\mathrm{d}t = \frac{9RT}{E_z}\left(\frac{T}{\theta_D}\right)^3 \int_0^{\theta_D/T}\frac{x^3}{e^x - 1}\mathrm{d}x \quad (5)$$

here, z_i is the atomic effective coordination number, θ_D is the Debye temperature, E_{z_i} is the single bond energy, and $x = \theta_D/T$ is the reduced form of the temperature. When the external temperature is greater than the Debye temperature, the specific heat C_v is approximately equal to a constant value of $3R$, where R represents the ideal gas constant. The atomic cohesive energy E_z

$= z_i E_{z_i}$ is the only adjustable parameter for the calculation of the thermal excitation of a given sample.

2.4. Photon and phonon thermal relaxation

We found the following proportional relationship for phonons and photons with respect to bond length and bond energy:

$$\begin{cases} \dfrac{\Delta\omega(T)}{\Delta\omega(T_0)} = \dfrac{d_{z_b}}{d(T)}\left[\dfrac{E(T)}{E_{z_b}}\right]^{1/2} \\ \dfrac{E_g(T)}{E_g(T_0)} = \dfrac{E(T)}{E_{z_b}} \end{cases} \quad (6)$$

where $\omega(T)$ is the measured value for the Raman frequency, $\Delta\omega(T) = \omega(T) - \omega(1)$ is the variation of the Raman frequency, $\omega(1)$ denotes the vibration frequency of a dimer, which comes from the Raman frequency of the reference point $\omega(0)$. Here, the reference frequency can vary with an incident laser wavelength, but the resulting shift is independent of the incident laser energy. Furthermore, $d(T)$ and $E(T)$ denote the bond length expansion and bond energy weakening with increase in temperature, respectively. Therefore, the Raman frequency and bandgap energy of these 2D films can be expressed as a function of bond length and bond energy for thermal excitation.

Combining eqn (1) to eqn (6), the thermal relaxation of the Raman frequency and bandgap energy can be expressed as:

$$\begin{cases} \dfrac{\Delta\omega(T)}{\Delta\omega(T_0)} = \left[1 - \dfrac{\int_0^T \eta(t)\mathrm{d}t}{E_z}\right]^{1/2} \exp\left(\int_0^T a(t)\mathrm{d}t\right) \\ \dfrac{E_g(T)}{E_g(T_0)} = 1 - \dfrac{\int_0^T \eta(t)\mathrm{d}t}{E_z} \end{cases} \quad (7)$$

According to eqn (7), the atomic cohesive energy is the only adjustable parameter for the calculation of the temperature-dependent Raman shift and bandgap energy. Because the thermal expansion coefficient $\alpha(t)$ is a very small value, about 10^{-6} K^{-1}, the following is valid: $1 + \int_0^T \alpha(t)\mathrm{d}t \leq 1 + 0.05$. Therefore, we can neglect the effects of thermal expansion on the temperature dependence of the Raman shift. Here, a proportional relationship was established to be studied between the temperature dependence of the Raman shift and bandgap energy because the exact values of the implied constants in the expression cannot reveal the relative variation in the respective physical quantities. The main objective of our study was to determine the bond contributions to electron and phonon spectroscopy and to extract the quantitative information from complex measurements carried out by other researchers.

3. Results and discussion

3.1. The vibrational modes of M-(X, X_2)

The interatomic force of M(X, X_2) is made up of covalent bonds and the van der Waals (VDW) forces. Strong covalent bonds provide the in-plane stability to 2D films, whereas relatively weak VDW forces are sufficient to keep the stack together. In Fig. 1, the dotted line denotes the weakening of the interlayer VDW force; the purple spheres are metal atoms; the green balls are group VIA atoms. Fig. 1(a) shows the two Raman active vibration modes of MX_2. E^1_{2g} is the in-of-plane vibration mode, which comes from the opposite direction of the vibration between two X atoms and intermediate M atoms. A_{1g} is the out-of-plane vibration mode, which is derived from the opposite direction of the vibration of two X atoms in a unit cell. Contrastingly, the MX films show out-of-plane modes (A^3_g) and in-plane modes (B_{3g}) (Fig. 1(b)) because MX shows wrinkled honeycomb structures, which is different from the hexagonal honeycomb structure of MX_2. The vibration modes of M(X, X_2) can not only be used to identify various nanomaterials but also provide the necessary basis for the study of the temperature dependence of the Raman shift of these 2D films.

3.2. Thermal relaxation of Raman shifts

Fig. 2 and 3 depict the BOLS reproduction observation results of the temperature-dependent A_{1g} modes and E^1_{2g} modes of MX_2,

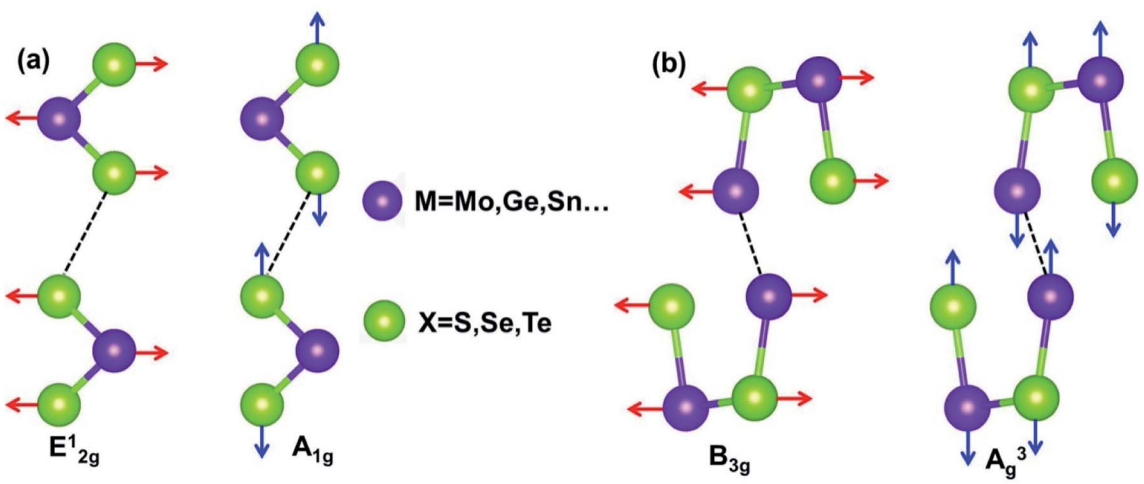

Fig. 1 The schematic of the main vibrational modes for nanostructure of (a) MX_2 (ref. 47) and (b) MX.[33]

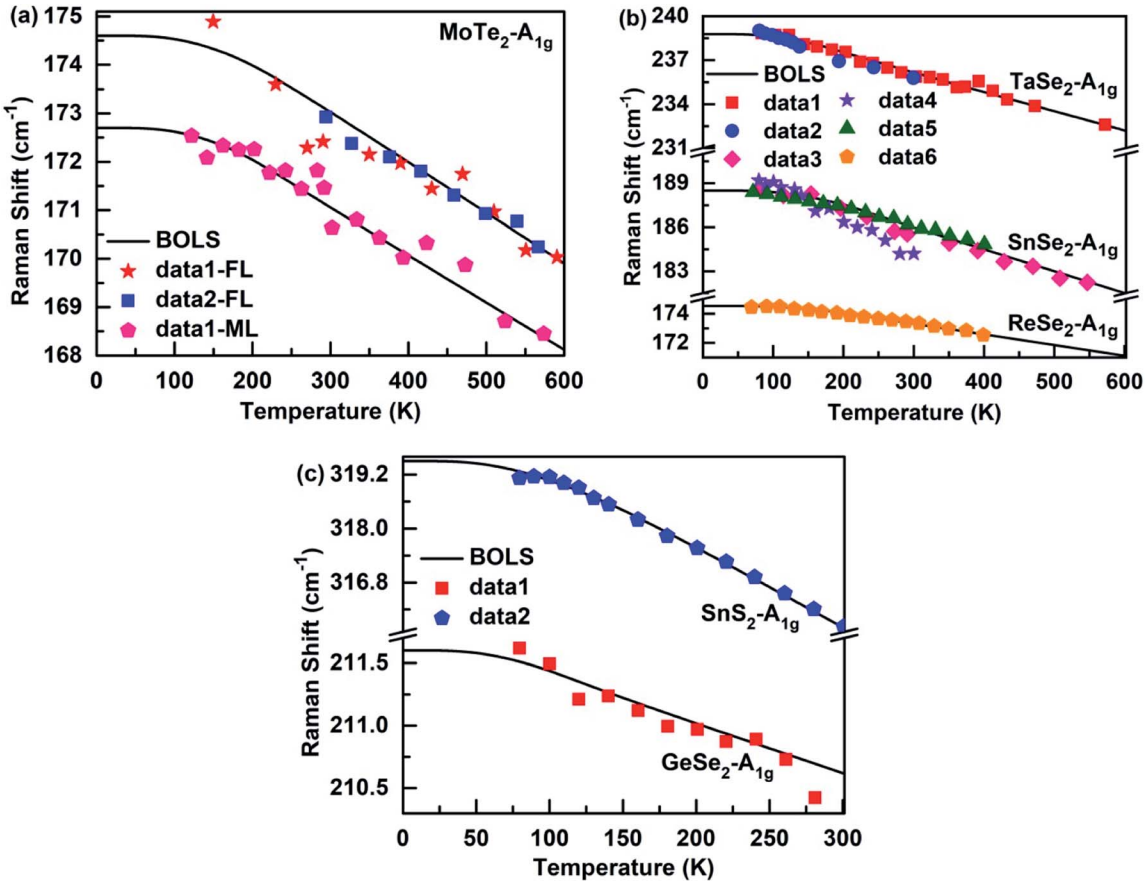

Fig. 2 The BOLS reproduction of the measured Raman A_{1g} modes for (a) few-layer[48,49] (FL) and monolayer[48] (ML) $MoTe_2$, (b) (Ta, Sn, Re)-Se_2,[50–54] and (c) (Sn, Ge)-(S_2, Se_2).[44,54]

respectively. The trends of all E^1_{2g} and A_{1g} modes turn gradually from nonlinear to linear during heating because the specific heat is $\eta(t) \propto T^3$ at low temperatures, due to which the Raman shift varies slowly with temperatures. However, the specific heat $\eta(t) \approx 3R$ (R is the ideal gas constant) at high temperatures, so the Raman shift display a linear decrease with the increase in temperature. Thus, the bond relaxation theory confirms that the Debye temperature determines the nonlinear range of the Raman shift at low temperatures. By calculating the temperature dependence of the Raman shift of MX_2, the Debye temperature (θ_D), the referential frequency $\omega_L(1)$ (L denote A_{1g} and E^1_{2g} modes), and atomic cohesive energy (E_z) can be listed in Table 1. These parameters are essential for calculating the temperature-dependent Raman shift of these 2D films.

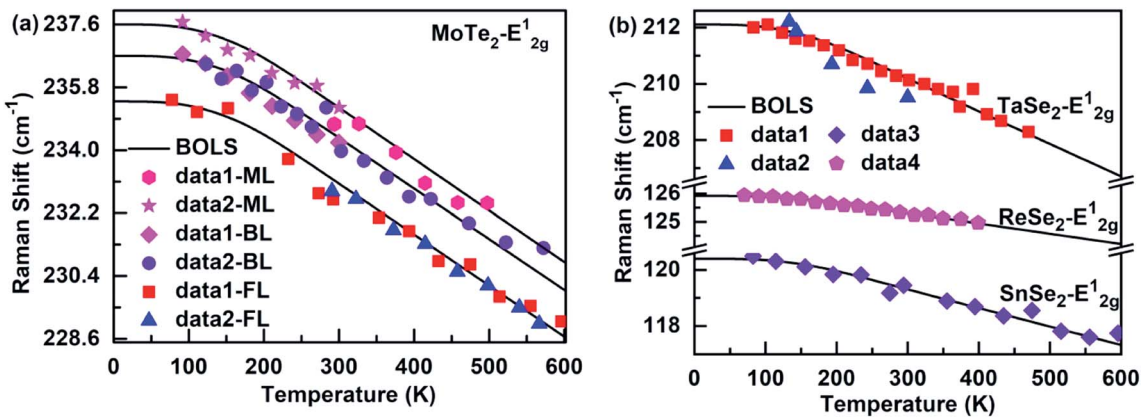

Fig. 3 Theoretical reproduction of the measured Raman E^1_{2g} modes for (a) monolayer[32,49] (ML), bilayer[32,48] (BL), and few-layer[48,49] (FL) $MoTe_2$, (b) (Ta, Sn, Re)-Se_2.[50–53]

Table 1 The referential frequency ($\omega_A(1)$ and $\omega_E(1)$), bulk bandgap energy (E_0), Debye temperature (θ_D), and cohesive atomic energy (E_z) were used to calculate the temperature dependence of the Raman shift and bandgap energy of M(X, X_2)

Stimuli	$\omega_A(1)$ (cm^{-1})	$\omega_E(1)$ (cm^{-1})	E_0 (eV)	E_z (eV)	θ_D (K)
$ReSe_2$	171.12	124.91	0.68	3.39	181 (ref. 25)
$TaSe_2$	232.12	206.73	—	5.23	150 (ref. 40)
$MoTe_2$	168.12[a]/169.80[c]	228.66[a]/230.01[b]/232.82[c]	0.58	4.22	169 (ref. 41)
$SnSe_2$	181.11	117.32	0.53	4.45	170 (ref. 42)
SnS_2	293.52	—	4.16	3.51	136 (ref. 43)
$GeSe_2$	198.52	—	1.21	2.29	180 (ref. 44)
SnSe	133.85[d]	88.46[e]	0.49	0.83	204 (ref. 33)
SnS	150.13[d]	84.96[e]	0.69	0.80	270 (ref. 45)
GeSe	175.62[d]	135.86[e]	0.65	0.69	214 (ref. 46)

[a] Monolayer of the nanomaterials. [b] Bilayer of the nanomaterials. [c] Few-layer of the nanomaterials. [d] A_g^3 modes. [e] B_{3g} modes.

According to eqn (7), the physical mechanism of the temperature-dependent Raman shift originates from the thermal excitation-induced bond length expansion and bond energy weakening.

Fig. 4 shows the BOLS approximation calculated temperature-dependent A_g^3 and B_{3g} modes of the MX films. The referential frequency ω_L (1) (L denote A_g^3 and B_{3g} modes), Debye temperature θ_D, and atomic cohesive energy E_z, which is hardly possible using the Varshni's semiempirical relationship and the Grüneisen model, is calculated in Table 1. From the table, it is clear that the Debye temperature for the SnS films was greater than for SnSe and GeSe, so the low-temperature nonlinear range of the former was distinctly larger than the latter. Thus, the results indicate that the Debye temperature determines the nonlinear range of the Raman shift of these 2D films at low temperatures.

3.3. E_z resolved a linear behavior at high temperatures

We first studied the temperature-dependent Raman shift of the monolayer (ML), bilayer (BL), and few-layer (FL) of the $MoTe_2$ film, which is applicable to the BOLS approximation as well, see Fig. 2(a) and 3(a). The BOLS approximation demonstrates that the atoms under coordination shorten the bond length and strengthen the bond energy, which means that the E_{2g}^1 modes experience a blue shift, and the A_{1g} modes undergo a redshift as the atomic layer number decreases. This was found to be similar to the layer number dependent Raman shift of MoS_2.[39] As a result, when there was no thermal stimulus, the phonon frequency of the few-layers of the A_{1g} modes of $MoTe_2$ was larger than that of the monolayer, but the phonon frequency of the E_{2g}^1 modes follows the opposite trend: $\omega_{ML} > \omega_{BL} > \omega_{FL}$. In addition, since $MoTe_2$ with a different atomic layer number had the same atomic cohesive energy, it shows the same behavior at high temperatures. Therefore, the BOLS approximation can resolve not only the layer number effect of the Raman shift of $MoTe_2$ film but can also clarify its temperature dependence.

Moreover, the atomic cohesive energy E_z determines the linear behavior at high temperatures of the temperature-dependent Raman shift for different nanomaterials in the same temperature range. When the temperature changes from 0 to 600 K, the atomic cohesive energy (see-Table 1) shows the following relationships: $E_{z\text{-}TaSe_2}$ (5.23 eV) > $E_{z\text{-}SnSe_2}$ (4.45 eV) > $E_{z\text{-}MoTe_2}$ (4.22 eV) > $E_{z\text{-}ReSe_2}$ (3.39 eV). Compared to the other three materials, $TaSe_2$ exhibit the largest linear behavior at high temperatures, so the rate of decrease in the Raman shift is the fastest for continuous heating. In addition, as shown in Fig. 2(c), the behavior for SnS_2

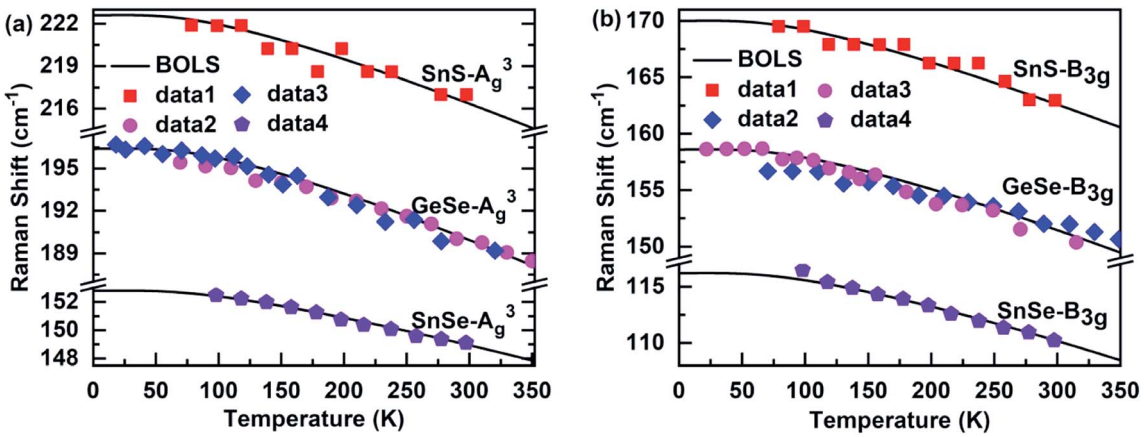

Fig. 4 Theoretical reproduction of the measured Raman (a) A_g^3 and (b) B_{3g} modes of SnS,[55] SnS,[30] and GeSe[56,57] films.

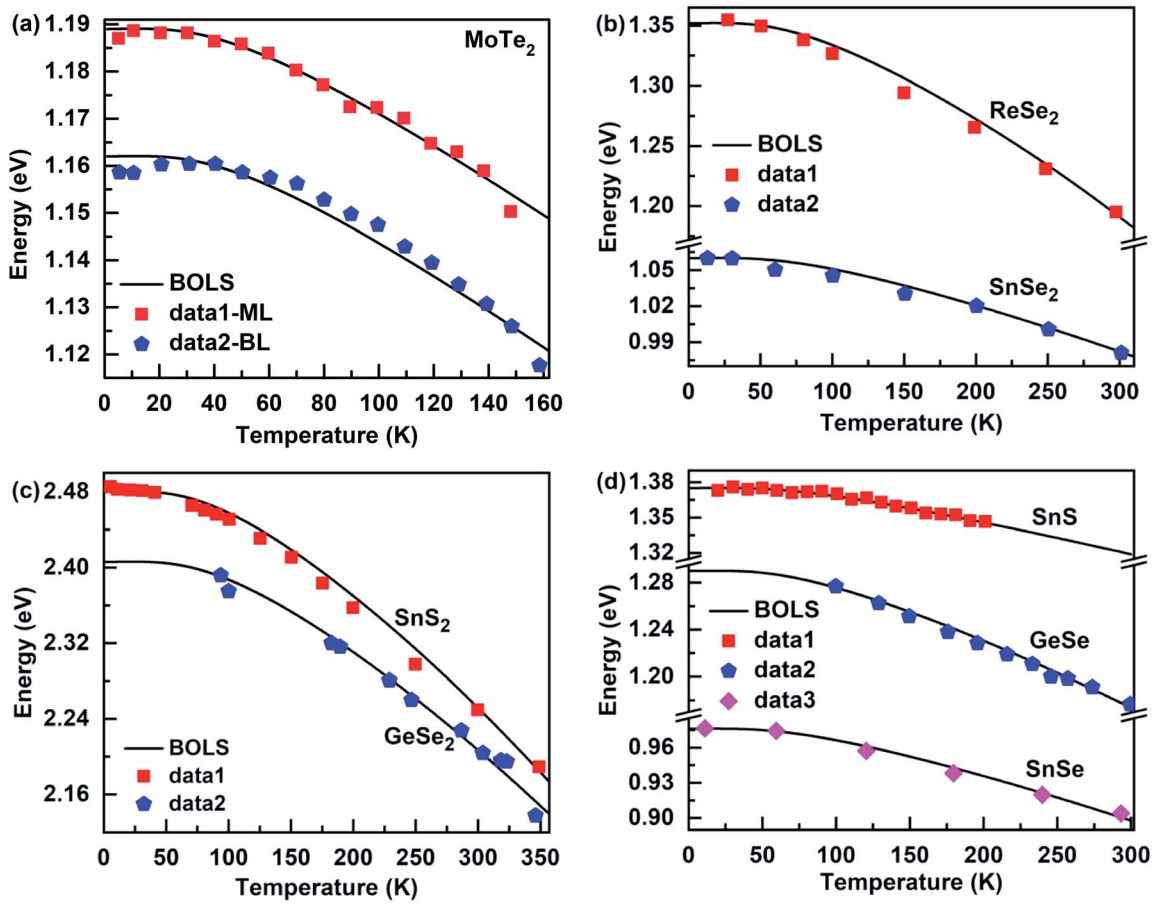

Fig. 5 Theoretical reproduction of the measured bandgap energy for (a) monolayer[23] (ML) and bilayer[23] (BL) $MoTe_2$, (b) $ReSe_2$ (ref. 25) and $SnSe_2$ (ref. 42), (c) SnS_2 (ref. 58) and $GeSe_2$ (ref. 59) and (d) (Sn, Ge)-(S, Se).[24,60,61]

at high temperatures was clearly larger than that for $GeSe_2$ for temperatures between 0 and 300 K. So, the order of their atomic cohesive energy calculated using the bond relaxation theory was $E_{z\text{-}SnS_2}$ (3.51 eV) > $E_{z\text{-}GeSe_2}$ (2.29 eV). A similar situation occurs for the Raman shift temperature dependence of SnS, SnSe, and GeSe. The agreement between the BOLS calculations and the experimental measurements confirms that the atomic cohesive energy E_z governs the behavior at high temperatures for thermal relaxation in these Raman spectroscopies.

3.4. Thermal relaxation of bandgap energy

The bandgap energy of the 2D nanomaterials is an important foundation for its applications in semiconductors and opto-electronic devices. Because the self-heating of the device is unavoidable, when an electronic equipment is used, this directly affects the bandgap energy of nanomaterials. This means it is important to understand the physical mechanism of the temperature-dependent of the bandgap energy of nano-materials. According to eqn (7), the thermal excitation increases the bond energy, which causes the thermal softening of the bandgap energy of these 2D film materials (see Fig. 5). The Debye temperature determines the nonlinear range at low temperatures, while the atomic cohesive energy governs the linear behavior at high temperatures, which is similar to the temperature dependence of the Raman shift of these 2D films. The BOLS approximation derived both atomic cohesive energy E_z and bulk bandgap energy E_0, which were used to calculate the temperature dependence of the bandgap energy of these 2D films (see Table 1). Thus, these results not only show the reliability of the bond relaxation theory when the temperature dependence of bandgap energy was calculated but also confirm that the Debye temperature and the atomic cohesive energy play an important role in the thermal softening of the bandgap energy.

4. Conclusion

In summary, we have investigated in detail the temperature dependence of the Raman shift and bandgap energy for M(X, X_2) using the BOLS approximation. The thermal softening of the Raman shift was caused by bond length elongation and bond energy expansion; the photon energy originates from the thermal excitation-induced weakening of the bond energy. The good agreement between the theoretical predictions and the experimental observations confirms that the Debye temperature determines the nonlinear range at low temperatures, while the atomic cohesive energy governs the linear behavior at high

temperatures for the thermal relaxation of the photon and phonon spectroscopy. Therefore, this study confirms the value of the bond relaxation theory, which enables the extraction of the quantitative information of bond length and bond energy from electron spectroscopy and phonon spectroscopy. The research method described in this study offers both new insight and effective tools for further exploring the thermal excitation behavior of other 2D films.

Conflicts of interest

There are no conflicts to declare.

Acknowledgements

This study was kindly supported by the National Natural Science Foundation of China (No.: 41425014), Key Laboratory Project of Jiangxi Province (No.: 20171BCD40010) and Two 1000 Talents Plan Project of Jiangxi Province (No.: S2018CQKJ0755).

References

1 K. S. Novoselov, A. K. Geim, S. V. Morozov, D. Jiang, Y. Zhang, S. V. Dubonos, I. V. Grigorieva and A. A. Firsov, *Science*, 2004, **306**, 666–669.
2 N. R. Pradhan, D. Rhodes, S. Feng, Y. Xin, S. Memaran, B.-H. Moon, H. Terrones, M. Terrones and L. Balicas, *ACS Nano*, 2014, **8**, 5911–5920.
3 F. Xia, H. Wang, D. Xiao, M. Dubey and A. Ramasubramaniam, *Nat. Photonics*, 2014, **8**, 899.
4 X. Wang, B. Liu, Q. Wang, W. Song, X. Hou, D. Chen, Y. b. Cheng and G. Shen, *Adv. Mater.*, 2013, **25**, 1479–1486.
5 O. Lopez-Sanchez, D. Lembke, M. Kayci, A. Radenovic and A. Kis, *Nat. Nanotechnol.*, 2013, **8**, 497.
6 E. Zhang, P. Wang, Z. Li, H. Wang, C. Song, C. Huang, Z.-G. Chen, L. Yang, K. Zhang and S. Lu, *ACS Nano*, 2016, **10**, 8067–8077.
7 B. Mukherjee, Z. Hu, M. Zheng, Y. Cai, Y. P. Feng, E. S. Tok and C. H. Sow, *J. Mater. Chem.*, 2012, **22**, 24882–24888.
8 X. Luo, F. Chen, J. Zhang, Q. Pei, G. Lin, W. Lu, Y. Han, C. Xi, W. Song and Y. Sun, *Appl. Phys. Lett.*, 2016, **109**, 102601.
9 J. Zhang, E. Sun, X. Feng, H. Liu, S. A. Redfern, V. Kanchana, G. Liu and H. Wang, *Phys. Chem. Chem. Phys.*, 2018, **20**, 29472–29479.
10 Y.-M. Zhang, J.-Q. Fan, W.-L. Wang, D. Zhang, L. Wang, W. Li, K. He, C.-L. Song, X.-C. Ma and Q.-K. Xue, *Phys. Rev. B*, 2018, **98**, 220508.
11 S. H. Choi and Y. C. Kang, *Nano Res.*, 2015, **8**, 1595–1603.
12 M.-Z. Xue, J. Yao, S.-C. Cheng and Z.-W. Fu, *J. Electrochem. Soc.*, 2006, **153**, A270–A274.
13 S. R. Suryawanshi, S. S. Warule, S. S. Patil, K. R. Patil and M. A. More, *ACS Appl. Mater. Interfaces*, 2014, **6**, 2018–2025.
14 M. A. Franzman, C. W. Schlenker, M. E. Thompson and R. L. Brutchey, *J. Am. Chem. Soc.*, 2010, **132**, 4060–4061.
15 L.-D. Zhao, S.-H. Lo, Y. Zhang, H. Sun, G. Tan, C. Uher, C. Wolverton, V. P. Dravid and M. G. Kanatzidis, *Nature*, 2014, **508**, 373.
16 A. Grant, T. Griffiths, G. Pitt and A. Yoffe, *J. Phys. C: Solid State Phys.*, 1975, **8**, L17.
17 C. Ruppert, O. B. Aslan and T. F. Heinz, *Nano Lett.*, 2014, **14**, 6231–6236.
18 N. R. Pradhan, C. Garcia, B. Isenberg, D. Rhodes, S. Feng, S. Memaran, Y. Xin, A. McCreary, A. R. H. Walker and A. Raeliarijaona, *Sci. Rep.*, 2018, **8**, 12745.
19 J. M. Gonzalez and I. I. Oleynik, *Phys. Rev. B*, 2016, **94**, 125443.
20 Y. Zhang, B. Shang, L. Li and J. Lei, *RSC Adv.*, 2017, **7**, 30327–30333.
21 G. Shi and E. Kioupakis, *J. Appl. Phys.*, 2015, **117**, 065103.
22 R. Fei, W. Li, J. Li and L. Yang, *Appl. Phys. Lett.*, 2015, **107**, 173104.
23 I. G. Lezama, A. Arora, A. Ubaldini, C. Barreteau, E. Giannini, M. Potemski and A. F. Morpurgo, *Nano Lett.*, 2015, **15**, 2336–2342.
24 T. Raadik, M. Grossberg, J. Raudoja, R. Traksmaa and J. Krustok, *J. Phys. Chem. Solids*, 2013, **74**, 1683–1685.
25 C. Ho, P. Liao, Y. Huang, T.-R. Yang and K. Tiong, *J. Appl. Phys.*, 1997, **81**, 6380–6383.
26 S. Logothetidis, P. Lautenschlager and M. Cardona, *Phys. Rev. B: Condens. Matter Mater. Phys.*, 1986, **33**, 1110.
27 X. Liu, G. Zhang, Q.-X. Pei and Y.-W. Zhang, *Appl. Phys. Lett.*, 2013, **103**, 133113.
28 W. Li, J. Carrete and N. Mingo, *Appl. Phys. Lett.*, 2013, **103**, 253103.
29 S. Jiang, L. Zhao, Y. Shi, C. Xie, N. Zhang, Z. Zhang, Y. Huan, P. Yang, M. Hong and X. Zhou, *Nanotechnology*, 2018, **29**, 204003.
30 S. Luo, X. Qi, H. Yao, X. Ren, Q. Chen and J. Zhong, *J. Phys. Chem. C*, 2017, **121**, 4674–4679.
31 J. Joshi, I. R. Stone, R. Beams, S. Krylyuk, I. Kalish, A. V. Davydov and P. M. Vora, *Appl. Phys. Lett.*, 2016, **109**, 031903.
32 J. Park, Y. Kim, Y. I. Jhon and Y. M. Jhon, *Appl. Phys. Lett.*, 2015, **107**, 153106.
33 F. Liu, P. Parajuli, R. Rao, P. Wei, A. Karunarathne, S. Bhattacharya, R. Podila, J. He, B. Maruyama and G. Priyadarshan, *Phys. Rev. B*, 2018, **98**, 224309.
34 C. W. Li, J. Hong, A. F. May, D. Bansal, S. Chi, T. Hong, G. Ehlers and O. Delaire, *Nat. Phys.*, 2015, **11**, 1063.
35 X. Liu, X. Zhang, M. Bo, L. Li, H. Tian, Y. Nie, Y. Sun, S. Xu, Y. Wang and W. Zheng, *Chem. Rev.*, 2015, **115**, 6746–6810.
36 X. Yang, C. Peng, L. Li, M. Bo, Y. Sun, Y. Huang and C. Q. Sun, *Prog. Solid State Chem.*, 2019, **55**, 20–66.
37 G. White, in *Physics in Australia: a review by the National Committee for Physics*, 1981.
38 C. Q. Sun, *Springer Ser. Chem. Phys.*, 2014, **108**, 807.
39 Y. Liu, M. Bo, Y. Guo, X. Yang, Z. Xi, C. Q. Sun and Y. Huang, *J. Raman Spectrosc.*, 2017, **48**, 592–595.
40 M. Naito and S. Tanaka, *Physica B*, 1981, **105**, 136–140.
41 S. Helmrich, R. Schneider, A. W. Achtstein, A. Arora, B. Herzog, S. M. D. Vasconcellos, M. Kolarczik, O. Schoeps, R. Bratschitsch and U. Woggon, *2D Mater.*, 2018, **5**, 045007.
42 P. Manou, J. Kalomiros, A. Anagnostopoulos and K. Kambas, *Mater. Res. Bull.*, 1996, **31**, 1407–1415.

43 A. Shafique, A. Samad and Y.-H. Shin, *Phys. Chem. Chem. Phys.*, 2017, **19**, 20677–20683.
44 X. Zhou, X. Hu, S. Zhou, Q. Zhang, H. Li and T. Zhai, *Adv. Funct. Mater.*, 2017, **27**, 1703858.
45 Y. M. Han, J. Zhao, M. Zhou, X. X. Jiang, H. Q. Leng and L. F. Li, *J. Mater. Chem. A*, 2015, **3**, 4555–4559.
46 M. Sist, C. Gatti, P. Nørby, S. Cenedese, H. Kasai, K. Kato and B. B. Iversen, *Chem.–Eur. J.*, 2017, **23**, 6888–6895.
47 P. Hajiyev, C. Cong, C. Qiu and T. Yu, *Sci. Rep.*, 2013, **3**, 2593.
48 D. J. Late, *Applied Materials Today*, 2016, **5**, 98–102.
49 H. Zhang, W. Zhou, X. Li, J. Xu, Y. Shi, B. Wang and F. Miao, *Appl. Phys. Lett.*, 2016, **108**, 091902.
50 J. Tsang, J. Smith Jr and M. Shafer, *Solid State Commun.*, 1978, **27**, 145–149.
51 Z. Yan, C. Jiang, T. Pope, C. Tsang, J. Stickney, P. Goli, J. Renteria, T. Salguero and A. Balandin, *J. Appl. Phys.*, 2013, **114**, 204301.
52 A. Taube, A. Łapińska, J. Judek and M. Zdrojek, *Appl. Phys. Lett.*, 2015, **107**, 013105.
53 A. S. Pawbake, A. Date, S. R. Jadkar and D. J. Late, *ChemistrySelect*, 2016, **1**, 5380–5387.
54 S. V. Bhatt, M. Deshpande, V. Sathe and S. Chaki, *Solid State Commun.*, 2015, **201**, 54–58.
55 J. Xia, X.-Z. Li, X. Huang, N. Mao, D.-D. Zhu, L. Wang, H. Xu and X.-M. Meng, *Nanoscale*, 2016, **8**, 2063–2070.
56 T. Fukunaga, S. Sugai, T. Kinosada and K. Murase, *Solid State Commun.*, 1981, **38**, 1049–1052.
57 A. Taube, A. Łapińska, J. Judek, N. Wochtman and M. Zdrojek, *J. Phys. D: Appl. Phys.*, 2016, **49**, 315301.
58 L. A. Burton, T. J. Whittles, D. Hesp, W. M. Linhart, J. M. Skelton, B. Hou, R. F. Webster, G. O'Dowd, C. Reece and D. Cherns, *J. Mater. Chem. A*, 2016, **4**, 1312–1318.
59 L. Tichý and H. Ticha, *Mater. Lett.*, 1992, **15**, 198–201.
60 A. Elkorashy, *J. Phys. Chem. Solids*, 1989, **50**, 893–898.
61 S. Vlachos, A. Lambros, A. Thanailakis and N. Economou, *Phys. Status Solidi B*, 1976, **76**, 727–735.